MRI Reconstruction with Enhanced Self-Similarity Using Graph Convolutional Network

Qiaoyu Ma
Jimei University
Zongying Lai (zongyinglai@jmu.edu.cn)
Jimei University
Zi Wang
Xiamen University
Yiran Qiu
Jimei University
Biao Qu
Xiamen University
Haotian Zhang
Jimei University
Xiaobo Qu
Xiamen University

Research Article

Keywords: Graph convolutional network, deep learning, fast magnetic resonance imaging, image reconstruction

Posted Date: March 21st, 2023

DOI: https://doi.org/10.21203/rs.3.rs-2702846/v1

Additional Declarations: No competing interests reported.

MRI Reconstruction with Enhanced Self-Similarity Using Graph Convolutional Network

Qiaoyu Ma[1†], Zongying Lai[1†*], Zi Wang[2], Yiran Qiu[1], Biao Qu[3], Haotian Zhang[1], Xiaobo Qu[2]*

[1]School of Ocean Information Engineering, Jimei University, Xiamen, China

[2]Department of Electronic Science, Biomedical Intelligent Cloud R&D Center, Fujian Provincial Key Laboratory of Plasma and Magnetic Resonance, National Institute for Data Science in Health and Medicine, Xiamen University, Xiamen, China

[3]Department of Instrumental and Electrical Engineering, Xiamen University, Xiamen, China

*Corresponding author: zongyinglai@jmu.edu.cn (Zongying Lai), quxiaobo@xmu.edu.cn (Xiaobo Qu)

[†]*These authors contributed equally to this work.*

Submitted to *BMC Medical Imaging*

ABSTRACT

Background

Recent convolutional neural network (CNN) performs low-error reconstruction in fast magnetic resonance imaging (MRI). Most of them convolve the image with kernels and have successfully explored the local information. However, the non-local image information, which is embed among image patches that are relatively far from each other, may be lost since the convolution kernel size is usually small. We aim to incorporate a graph to represent non-local information, and improve the reconstructed images by Enhanced Self-Similarity Using Graph Convolutional Network (GCESS).

Methods

First, image is reconstructed into graph to extract the non-local self-similarity in the image. Second, GCESS uses graph convolution and spatial convolution to process the information in the image, so that local and non-local information can be effectively utilized. The network strengthens the non-local similarity between similar image patches while reconstructing images, making the reconstruction details more reliable.

Results

Experimental results on in vivo knee and brain data demonstrate that the proposed method achieves better artifacts suppression and details preservation than state-of-the-art methods, both visually and quantitatively. Under 1D Cartesian sampling with 4x acceleration (AF=4), the PSNR of knee data reached 34.19 dB, 1.05 dB higher than that of the compared methods; the SSIM achieved 0.8994, 2% higher than the compared methods. Similar results were obtained for the reconstructed images under other sampling templates as demonstrated in our experiment.

Conclusions

The proposed method successfully construct a hybrid graph convolution and spatial convolution network to reconstruct images. Along with the network training, the non-local self-similarities are enhanced, and will benefit the image details reconstruction. Experiments demonstrate that the proposed method outperforms the state-of-the-art reconstruction method in suppressing artifacts, as well as in preserving image details.

Keywords: Graph convolutional network, deep learning, fast magnetic resonance imaging, image reconstruction

Background

Magnetic resonance imaging (MRI) is an indispensable non-radiative medical imaging technology with excellent tissue resolution. However, due to the physical limit, its data acquisition is relatively long. Thus accelerating the data acquisition attracts great interest[1]. To achieve this goal, the representative methods include parallel imaging[2] and undersampling[1]. However, undersampling inevitably introduces image artifacts. Compressed sensing (CS)[1] remove these artifacts by constraining the image sparsity in a transform domain, especially under an adaptively trained sparse representations[3, 4]. To fit for a target image, a sparser representation can be obtained via self-learning the similar patches and greatly improve the reconstructed image[5-7]. Through the similar patches, two prior information could be learnt, including the non-local similarity and the way of sparsifying images. For example, the non-local total variation (NLTV)[7] explores the similarity by measuring Gaussian distance of image patches and use the weighted total variation to sparsity image pix. Patch-based non-local operator (PANO)[5] learns similarity through grouping similar patches of a pre-reconstruction of the target image and sparsify grouped patches with 3D wavelets. The graph-based redundant wavelet transform (GBRWT)[6], by viewing each patch as a node on a graph and the difference of image patch as the edge, the similarity is denoted as a shortest travel over the graph. The order of traveling each node (image patch) is also the order of sorting image pixels. Then, 1D wavelets is used to sparsify the sorted image pixels. All these methods requires a pre-reconstructed image to learn the similarity, thus the reconstruction may be unsatisfactory if the pre-reconstruction is not good under high acceleration factor of fast sampling[8].

Inspired by deep learning[9-11], early deep learning MRI reconstruction methods commonly utilize convolutional neural network (CNN) to perform the reconstruction[12, 13] and have achieved great success[14-23]. Unlike previous compressed sensing methods using the pre-defined sparsifying, deep learning methods enables convolution kernels learned from MRI image database. They take advantages of local spatial information of grid-like structure by the use of convolutional kernels

and have obtained good feature expression capacity. In recent years, DONet[24] learns multi-scale spatial-frequency features from both the real and imaginary components of MR data for fast parallel MRI image reconstruction, which enlarges the receptive field globally. DC-WCNN[25] use wavelet transform instead of pooling layer to extract multiple information in MRI images. These methods process and analyze image from a global perspective, but ignores the non-local self-similarity inner an image. Recently, the graph structure has become an important topic owing to its adjacency relation representation[26]. The graph is non-Euclidean data, and common CNN architectures cannot process this kind of data. Therefore, deep networks that can be directly applied to graphs have attracted great attention[26-29]. Similarity-Guided Graph Neural Network (SGGNN)[30] creates a graph to represent the pairwise image relationships and utilized the similarity between images to learn the edge weights with rich labels of gallery instance pairs directly. We are motivated to represent non-local self-similarity of MRI image as a graph, in which the most adjacent nodes with similar structures can be used to further remove artifacts and preserve details for the target node.

In this work, we propose a Graph Convolution network with Enhanced Self-Similarity (GCESS) to reconstruct MRI images from undersampled k-space data. We use graph convolutions to filter patches, and reconstructed images are recomposed from these filtered patches. As the network training, updated graph filters and enhanced graph weights are obtained. An accurate estimation of self-similarity is important for graph convolutional neural networks. Ideally, optimal self-similarity should be estimated on a fully sampled image, which is not available in fast MRI. To alleviate this problem, we propose to estimate self-similarity from a pre-reconstructed image obtained by a conventional reconstruction method SPIRiT[31]. We also include a spatial convolution process to effectively utilize local and non-local simultaneouly for image reconstruction. Our main contributions are: 1) Non-local self-similarity guided graph convolution is combined with local spatial convolution for improved MRI reconstructions. 2) Extensive results on in vivo datasets show that, the proposed GCESS provides better reconstruction performance than state-of-the-art methods visually and quantitatively, especially in artifact suppression and detail preservation.

Methods

In this section, we review the basic MRI reconstruction model[32], and then propose the GCESS network. This network incorporates non-local self-similarities and local feature which are respectively represented by graph convolution and local spatial convolution process for MRI images. First, a patch graph connects the non-local information of MRI images to enhance the self-similarity, where graph nodes are vectorized image patches and edge weights represent differences between patches. Then, graph convolutional kernels are updated by the network training process and apply to renovate node features. During the training process, the interconnected weight between similar image patches is further enhanced and feeds back to the graph convolution filter. The graph convolution and spatial convolution are combined to form our GCESS, which simultaneously takes advantage of non-local self-similarities and local information for improved MRI reconstruction.

When an image is sufficiently sparse in the transform domain, the theory of CS[1] enables accurate image recovery from limited measurement data. The basic MRI imaging model in CS can be written as [32]:

$$\min_{\mathbf{x}} \lambda \sum_{j=1}^{J} \left\| \mathbf{y}_j - \mathbf{F}_u \mathbf{C}_j \mathbf{x} \right\|_2^2 + R(\mathbf{x}), \tag{1}$$

where $\mathbf{x} \in £^N$ is the vectorization form of a reconstructed image, $\mathbf{y}_j \in £^M$ is the undersampled k-space data acquired from the j^{th} coil, $\mathbf{C}_j$ is the sensitivity map of j^{th} coil, $\mathbf{F}_u = \mathbf{UF} \in £^{M \times N}$ denotes the undersampled Fourier transform operator ($M < N$). $\|\cdot\|_2$ stands for l_2 norm which enforces the fidelity of the reconstruction to the measured k-space data. λ is a weight to balance the data consistenc and regularization term. $R(\mathbf{x})$ denotes the regularization term capturing the assumed model of the underlying in image, such as sparse transform and proximity to deep learning reconstructions. In this work, a deep network regularization term constrains local and non-local information will be introduced. We will start from the representation of non-local self-similarity in the following sections.

Graph Representation of Self-Similarities

The local and non-local information is vital to be constrained for MRI reconstructions. Local information is treated in the way of local spatial convolution like most methods[14-22]. To constrain non-local information with self-similarity, a patch graph is constructed to form a graph convolutional network. Graph nodes are vectorized image patches. Weights in a patch graph denote similarities between image patches. Graph network learning will enhance the non-local self-similarity in the image and update graph convolution filters.

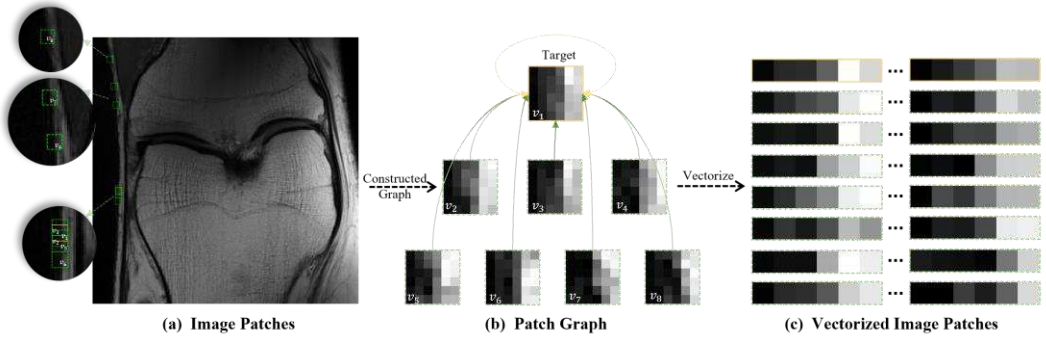

Fig. 1. The whole process of constructing a graph from an image. Representation of non-local self-similarity with a patch graph of fully sampled MRI image. The image patch bounded by the solid yellow line is set as the target image patch. Similar image patches are represented by green dotted lines distributed in the image. (a) the eight most similar image patches are found in the global image. (b) graph is constituted with a similar patch found in (a). (c) vectorized image patches (nodes).

Specifically, for every node (Target image patch) in the graph, we search the eight most similar image patches (Including self-connection) as the connected nodes. The patch graph is set as $\mathrm{G}(\mathrm{V},\mathrm{E})$ with N nodes $v_i \in \mathrm{V}$ and edges $(v_i, v_j) \in \mathrm{E}$, $i, j = 1,2,\mathrm{L}\ ,N$. Fig. 1(a)-(b) show that one target image patch (node v_1) connects with its most similar patches. The weight (Euclidean distance[33, 34] between v_i and v_j) on the edges $(v_i, v_j) \in \mathrm{E}$ constitute different adjacency matrix $\hat{\mathbf{A}} \in \mathbf{R}^{N\times N}$. Therefore, image patches with more similarities, which are not adjoined in the grid-like images, are connected by edges with small weights in the graph. These similarities will be enhanced by graph convolution filter update process to assist MRI reconstructions.

To enhance the pairwise relations of a node with adjacent nodes' information, the Gaussian function is utilized to weight all Euclidean distance[35]:

$$\mathbf{A}_{ij} = \exp\left(-\frac{\left\| v_i - v_j \right\|_2^2}{\sigma(\mathrm{V})^2} \right), \tag{2}$$

where $\sigma(\mathrm{V})$ is the standard deviation of the nodes. Gaussian function has normalization ability for weights which can avoid the filter from updating unnecessary dimensional gaps to reduce computational complexity. Obviously, with Gaussian function, the self-connected edge weight of target patch is 1. This process further enforces the most important weights.

A graph representing self-similarity is summarized in the Fig. 1. The connected patches share information, and can be aggregated to reconstruct the target patch. The selection of connected patches is affected by the reference image. Reference images with great artifact will make the selected connection not consistent with the true similar relationships. The comparison of undersampled similarity, reconstructed similarity and optimal similarity are shown in Fig. 2. Here, undersampled similarity means that similarity weights are calculated from undersampled image, reconstructed similarity means that similarity weights are calculated from image reconstructed by a conventional MRI reconstruction method, i.e. iterative Self-consistent Parallel Imaging Reconstruction (SPIRiT)[31], and optimal similarity means that similarity weights are calculated from fully sampled image. Adjacency weight is annotated on the graphic (Fig. 2) according to spatial position of image patches. The resulting chart shows that the similar relationship in the undersampled image is inconsistent with the optimal one. The similarity relationship is crucial in graph convolution which will be used to train graph convolution to facilitate the target image reconstruction. Therefore, the similarity weight calculated from a carefully pre-reconstructed image is designed to make the similarity weight be more consistent with optimal similarity, as shown in Fig. 2(b). The effect of similarity on the reconstruction results will be introduced in the next section.

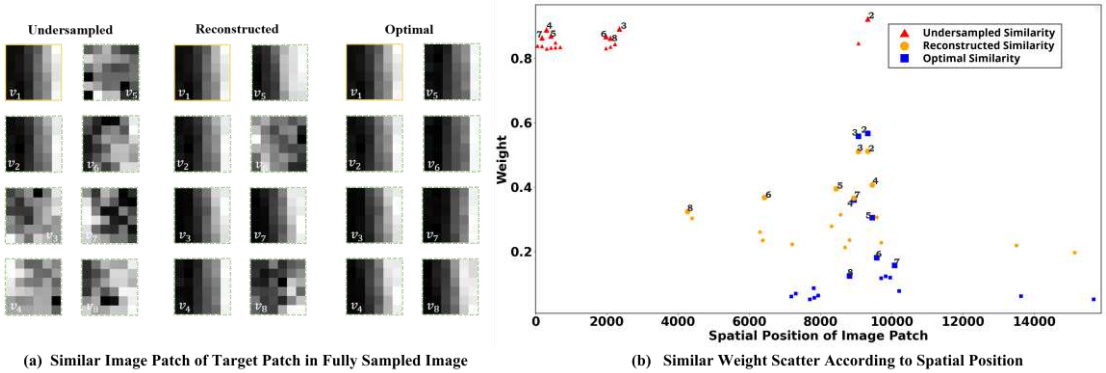

(a) Similar Image Patch of Target Patch in Fully Sampled Image (b) Similar Weight Scatter According to Spatial Position

Fig. 2. Selection of most seven similar connected patches in different reference image. (a) the target patch v1 and its seven most similar patches v_2-v_8 in undersampled, reconstructed and optimal similarity. To better see the difference, image patches are selected from fully sampled image. (b) similarity weights to the target patch in different references (self-connection is excluded). The seven most similar nodes emphasize with larger dots compared with others. Note: Optimal similarity means that weights are calculated from fully sampled image. Undersampled similarity means that weights are calculated from an undersampled image. Reconstructed similarity means that weights are calculated from image reconstructed by conventional parallel MRI methods.

Graph Convolution with Enhanced Self-similarity

The deep network regularization incorporates a graph convolution learning process using non-local similarity. In practice, non-local patch-pair similarities can be enhanced by the graph convolution, and can be utilized in the nodes' reconstruction. The nodes' feature in the graph is initialized as vectorized image patches. Adjacency matrix $\mathbf{A}$ corresponds to the measured similarity of each patch pair. In the graph, each node has one degree. The degree $\mathbf{D}_{ii} = \sum_{j}^{N} \mathbf{A}_{ij}$ $(i, j = 1, 2, \mathrm{L}\ , N)$ refers to the sum of the influence of the i-node on all graph nodes, and node degrees form a diagonal degree matrix, i.e. $\mathbf{D} = diag\left(\mathbf{D}_{ii}\right)$. The graph Laplacian is normalized $\mathbf{L} = \mathbf{I}_N - \mathbf{D}^{-\frac{1}{2}}\mathbf{A}\mathbf{D}^{-\frac{1}{2}} = \mathbf{U}\Lambda\mathbf{U}^T$, where $\mathbf{U}$ is the matrix of eigenvectors and Λ is a diagonal matrix of eigenvalues of the normalized graph Laplacian. The spectral graph convolution[26] can be used to study the non-local similarities represented by the graph,

$$\mathbf{g}_\theta * \mathbf{M} = \mathbf{U}\mathbf{g}_\theta\mathbf{U}^T\mathbf{M}, \tag{3}$$

where $\mathbf{M} \in \mathbf{R}^{N \times C}$ is a matrix of node features stacked by row. $\mathbf{U}^T\mathbf{M}$ is the Fourier transform of $\mathbf{M}$. $\mathbf{g}_\theta = diag(\theta)$ is a spectral filter parameterized by $\boldsymbol{\theta} \in \mathbf{R}^N$. Without loss of generality, scalar nodes are used instead to explain the proposed graph convolution process, and thus $\mathbf{m} \in \mathbf{R}^N$ is used instead of $\mathbf{M}$ in the following explanation. The $\mathbf{g}_\theta$ can be further understood as a function of the eigenvalues of $\mathbf{L}$, i.e. $g_\theta(\boldsymbol{\Lambda})$.

Computing the eigen-decomposition has low efficiency and high computational complexity. To circumvent this problem, it was suggested by Hammond et al.[36] that $g_\theta(\boldsymbol{\Lambda})$ can be well-approximated by a truncated expansion in terms of Chebyshev polynomials $T_k(\boldsymbol{\Lambda})$. The independent variables of $T_k(\boldsymbol{\Lambda})$ are required to be varied within the range $[-1, 1]$. In this case, the eigenvalues $\boldsymbol{\Lambda}$ are rescaled as $\tilde{\boldsymbol{\Lambda}} = (2/\lambda_{\max})\boldsymbol{\Lambda} - \mathbf{I}_N$, where $\lambda_{\max}$ denotes the largest eigenvalue of $\mathbf{L}$. $\lambda_{\max}$ approximately equals to 2, which can be expected that neural network parameters will adapt to this change in scale during training. The graph convolution with Chebyshev polynomial can be reformulated as

$$\mathbf{g}_\theta * \mathbf{m} = \mathbf{U}\mathbf{g}_{\theta'}(\tilde{\boldsymbol{\Lambda}})\mathbf{U}^T\mathbf{m} \approx \sum_{k=0}^{1} \theta'_k T_k(\tilde{\mathbf{L}})\mathbf{m} = \theta'_0\mathbf{m} + \theta'_1\tilde{\mathbf{L}}\mathbf{m}, \tag{4}$$

with rescaled normalized graph Laplacian $\tilde{\mathbf{L}} = (2/\lambda_{\max})\mathbf{L} - \mathbf{I}_N$. θ'_0 and θ'_1 are coefficients of Chebyshev polynomials. The 1st order Chebyshev polynomials are defined as $T_1(\tilde{\mathbf{L}}) = 1 + \tilde{\mathbf{L}}$. Setting the parameters to the same value $\theta' = \theta'_0 = -\theta'_1$, the equation (4) is further simplified as

$$\mathbf{g}_\theta * \mathbf{m} = \theta'_0\mathbf{m} - \theta'_1\mathbf{D}^{-\frac{1}{2}}\mathbf{A}\mathbf{D}^{-\frac{1}{2}}\mathbf{m} = \theta'\left(\mathbf{I}_N + \mathbf{D}^{-\frac{1}{2}}\mathbf{A}\mathbf{D}^{-\frac{1}{2}}\right)\mathbf{m}. \tag{5}$$

The eigenvalue of $\mathbf{I}_N + \mathbf{D}^{-\frac{1}{2}}\mathbf{A}\mathbf{D}^{-\frac{1}{2}}$ is more than 1. Therefore, repeating this operation in the deep learning model will lead to numerical instability and explosion gradient. To alleviate these problems, $\mathbf{I}_N + \mathbf{D}^{-\frac{1}{2}}\mathbf{A}\mathbf{D}^{-\frac{1}{2}}$ is renormalized as $\tilde{\mathbf{D}}^{-\frac{1}{2}}\tilde{\mathbf{A}}\tilde{\mathbf{D}}^{-\frac{1}{2}}$. $\tilde{\mathbf{A}} = \mathbf{A} + \mathbf{I}_N$ is the adjacent matrix of graph that each node has self-connecting edge and $\tilde{\mathbf{D}}_{ii} = \sum_j \tilde{\mathbf{A}}_{ij}$ is the degree of i-th node. Then the graph convolution becomes

$$\mathbf{g}_\theta * \mathbf{m} \approx \theta'\tilde{\mathbf{D}}^{-\frac{1}{2}}\tilde{\mathbf{A}}\tilde{\mathbf{D}}^{-\frac{1}{2}}\mathbf{m}. \tag{6}$$

This formula realizes node feature filtering guided by similarity weight with a spectral graph convolution operation. Then the i-th node feature can be rewritten as:

$$\theta\left(\tilde{\mathbf{D}}^{-\frac{1}{2}}\tilde{\mathbf{A}}\tilde{\mathbf{D}}^{-\frac{1}{2}}\mathbf{m}\right)_i = \theta\sum_j^N \frac{\tilde{\mathbf{A}}_{ij}\mathbf{m}_{j\cdot}}{\sqrt{\tilde{\mathbf{D}}_{ii}\tilde{\mathbf{D}}_{jj}}}, \tag{7}$$

where $\tilde{\mathbf{D}}_{ii}$ denotes i-th node (Target node) degree and $\tilde{\mathbf{D}}_{jj}$ denotes j-th node degree in the graph. $\tilde{\mathbf{A}}_{ij}$ is the similarity weights between i-th and j-th node. The node features are updated by fusing most similar connected nodes with a graph convolution process. The non-local information is aggregated by selecting the most similarity weight through the graph. The larger weight of $\tilde{\mathbf{A}}_{ij}$ representing, the more similarities between nodes (v_i and v_j), and the greater contribution can be obtained in target node reconstruction. In order to reduce the interference of unimportant weights, except for the most similar weights, others are set to zero.

Simultaneously, through the implementation of network training, the target image can quickly obtain the information of image patches with strong similarity through the connection edge. In the process of graph convolution, the convolution kernel continuously adjusts its parameter weight through training, so as to adaptively control the information transfer between these image patches and the target one. Such adaptive adjustment can improve the aggregate reconstruction of target patches by connecting patches. In this way, the information gathered by convolution will further enhance the self-similarity in the image. The proposed feature updating is intuitive since the rich non-local information with enhanced self-similarity are effectively exploited. Using similarity weights to guide the refinement of the nodes' feature reconstruction will lead to the more accurate reconstructed feature. It is worth noting that filter θ adaptively performs weighting with the most similarity in the graph to update target node features for reconstruction more accurately.

Generalizing the graph filtering process to a signal $\mathbf{M} \in \mathbf{R}^{N\times C}$ with C input channels (A C-dimensional feature vector for every node):

$$\mathbf{Z} = \tilde{\mathbf{D}}^{-\frac{1}{2}}\tilde{\mathbf{A}}\tilde{\mathbf{D}}^{-\frac{1}{2}}\mathbf{M}\Theta, \tag{8}$$

where $\Theta \in \mathbf{R}^{C\times F}$ is filter parameter and $\mathbf{Z} \in \mathbf{R}^{N\times F}$ is feature matrix after convolution. This is also in line with practical MRI reconstruction, where noise and artifacts usually

contaminate image pixels. In this case, when patch nodes are used instead of scope pixel, edge weights calculation and the subsequent graph convolution will be insensitive to noise and artifacts. Then the aggregation of non-local information with self-similarity to reconstruct target image will be robust.

Graph Convolutional Network for MRI Reconstruction

A regularized MRI reconstruction framework incorporated graph convolution as the Graph Convolutional Network (GCN) can be formulated as:

$$\min_{\mathbf{x},\Theta} \lambda \sum_{j=1}^{J} \left\| \mathbf{y}_j - \mathbf{F}_u C_j \mathbf{x} \right\|_2^2 + \left\| \mathbf{x} - \mathrm{I}\left(\tilde{\mathbf{D}}^{-\frac{1}{2}} \tilde{\mathbf{A}} \tilde{\mathbf{D}}^{-\frac{1}{2}} \mathbf{M} \Theta \right) \right\|. \tag{9}$$

where $\mathrm{I}(\cdot)$ convert graph information back to image, named image transformer (Itrans). Since the k-space data are undersampled, no ground truth image is available to learn patch similarity. Here we use the pre-reconstructed image using SPIRiT[31] to learn patch similarity. The learned similarities are more consistent with the optimal similarity than those learned from undersampled image, which is clearly illustrated in Fig. 2 in previous section.

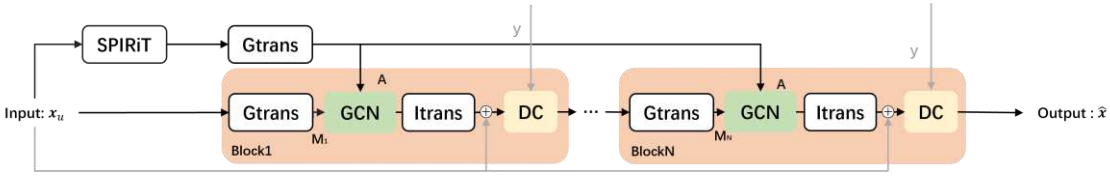

Fig. 3. This network block consists of GCN and DC parts, with the blocks cascaded. Graph transformer (Gtrans) and image transformer (Itrans) are the function of image-to-graph and graph-to-image, respectively. The adjacency matrix A and features M are obtained from the reconstructed image and the undersampled image respectively.

The flowchart of using GCN in a network to reconstruct MRI images is illustrated in Fig. 3. The Graph transformer (Gtrans) module in Fig. 3 transforms an image to be a graph, including graph nodes (patches) and graph weights (similarities). The flowed $\mathbf{A}$ from Gtrans denotes that graph weights flow into next module, and flowed $\mathbf{M}_i$ ($i = 1, \mathrm{L}, N$) from Gtrans denotes graph nodes (patches) flow into next module. Data consistency (DC) will be described in detail together with the proposed method in the following Section. E. The reconstructed images shown Fig. 4 and RLNE in Table 1

show the benefit of GCN. We use the relative ℓ_2 norm error (RLNE)[5] which is defined as:

$$RLNE = \left\| \mathbf{x} - \hat{\mathbf{x}} \right\|_2 / \left\| \mathbf{x} \right\|_2 , \tag{10}$$

where $\hat{\mathbf{x}}$ is the reconstructed image and $\mathbf{x}$ denotes the fully sampled image. Similarity calculated from undersampled image is denoted as GCN with undersampled similarity (UnGCN). Similarity calculated from pre-reconstructed image is denoted as GCN with reconstructed image (RecGCN). The number of blocks (Filter trainable parameters number is 64 × 36 × 2 × 10) is set to 10.

Table 1. Quantitative results (RLNE) of the compared method (Mean ± standard).

Method	AF=4 (1D Cartesian)		
	SPIRiT	UnGCN	**RecGCN**
RLNE×100	10.10 ± 1.16	9.80 ± 0.97	**8.55 ± 0.81**

As shown in Fig. 4, GCN with properly learned similarities shows an effective reconstruction of MRI images, which indicates that non-local information with self-similarities can be used to reconstruct target image patch effectively. When similarities are inaccurate, that is, only undersampled image can be used for calculation of similarity weights may cause the found connected patches to be vastly different, and hence degrade the reconstruction. Reconstructed image with UnGCN is degraded compared with reconstructed image with RecGCN. In the following experiments, similarities are calculated from the SPIRiT reconstructed image, considering the undersampled data in real applications.

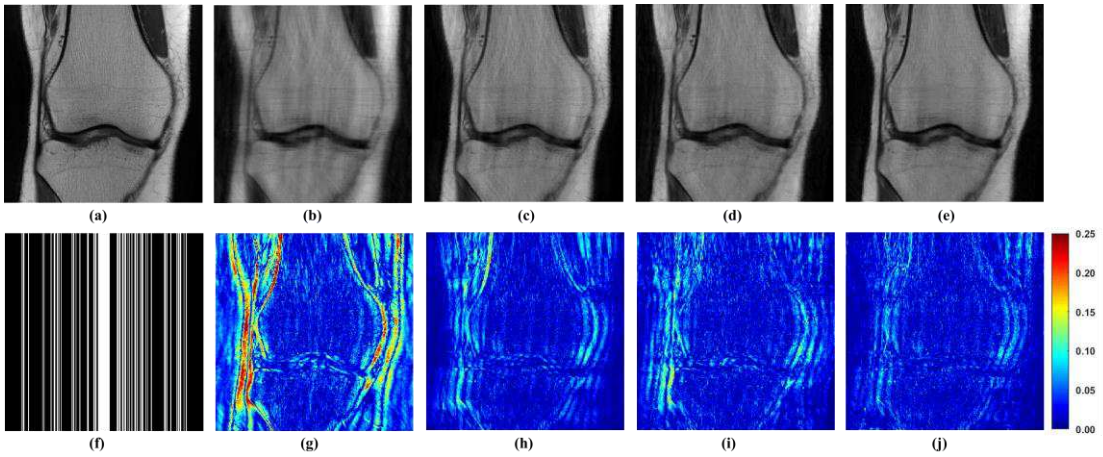

Fig. 4. The proposed GCN for MRI reconstructions. (a) is the fully sampled image. (b) is the undersampled image. (f) is the 1D Cartesian undersampling pattern with AF=4. (c)-(e) are reconstructed images by SPIRiT, UnGCN, and RecGCN, respectively. (g)-(j) are the corresponding error maps.

The Proposed GCESS for MRI Reconstruction

Ignore local context information in image domain is unwise for MRI reconstructions. We propose deep learning network GCESS to combine local information represented by CNN and non-local information grasped by GCN,

$$\min_{\mathbf{x},\boldsymbol{\Theta}} \lambda \sum_{j=1}^{J} \left\| \mathbf{y}_j - \mathbf{F}_u C_j \mathbf{x} \right\|_2^2 + \left\| \mathbf{x} - f\left(\mathbf{x}_u \middle| \boldsymbol{\Theta}\right) \right\|. \tag{11}$$

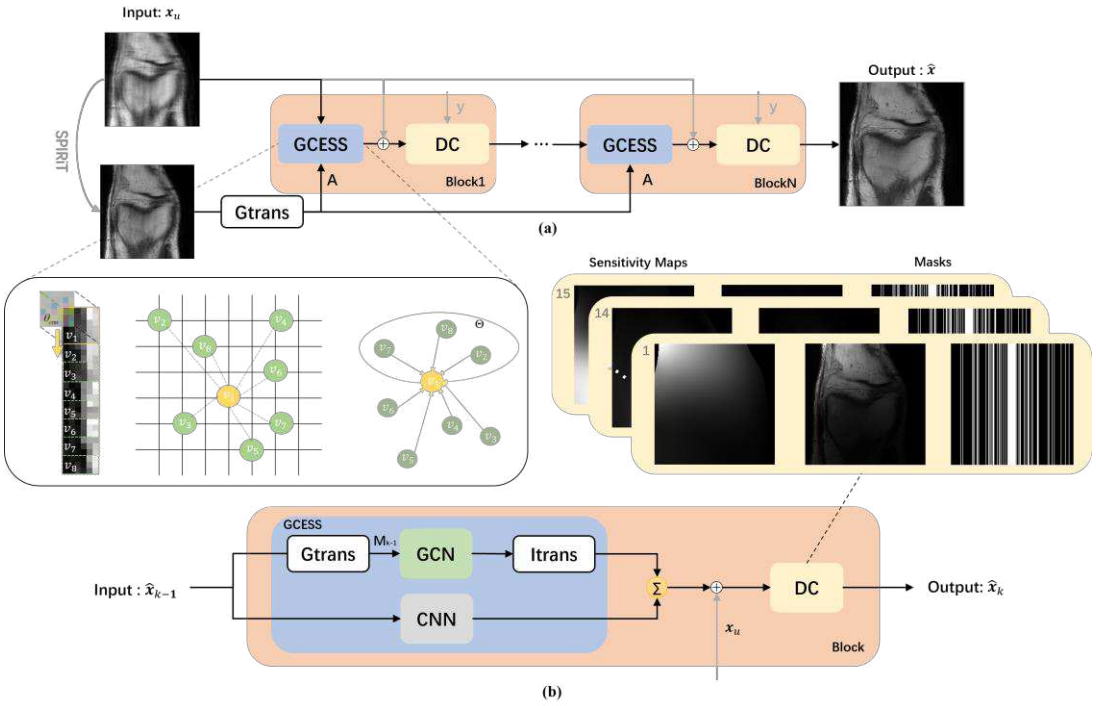

Fig. 5. The proposed GCESS for MRI reconstruction. (a) is the proposed network consisting of GCESS and DC, with blocks cascaded. The graph is learned from SPIRiT pre-reconstructed image. (b) is a detailed analysis of the main part of the network block.

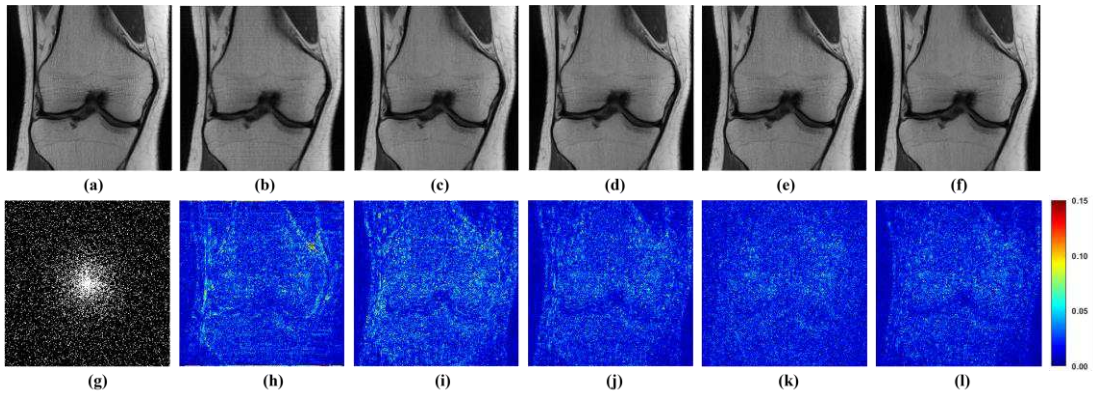

Fig. 6. The proposed GCESS network compared with state-of-the-art MRI reconstruction methods. (a) is the fully sampled image. The experiments correspond to a 2D random sampling with AF=8 as shown in (g). (b)-(f) are the images of reconstructed results by SPIRiT, IUNET, DCCNN, MoDL, and GCESS, respectively. (h)-(l) are the corresponding error maps. The PSNR of (b)-(f) are, 32.51, 29.04, 33.67, 33.99 and 34.42 dB, respectively.

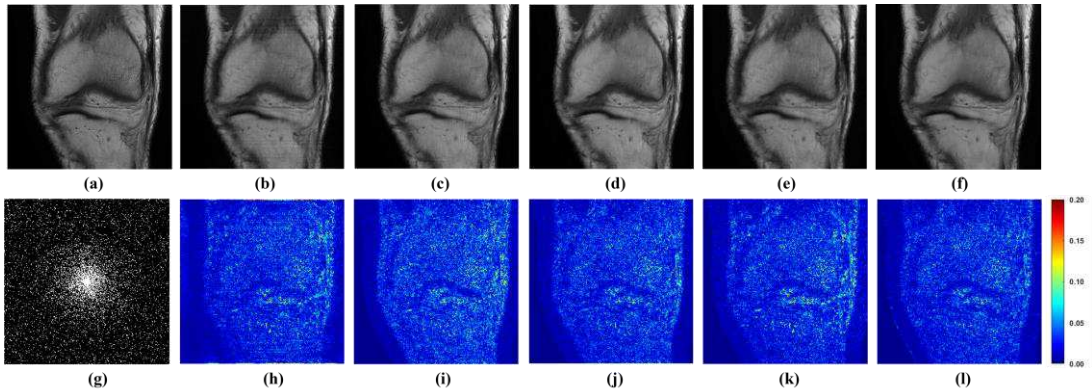

Fig. 7. The proposed GCESS network compared with state-of-the-art MRI reconstruction methods. (a) is the fully sampled image. The experiments correspond to a 2D random sampling with AF=10 as shown in (g). (b)-(f) are the images of reconstructed results by SPIRiT, Unet, DCCNN, MoDL, and GCESS, respectively. (h)-(l) are the corresponding error maps. The PSNR of (b)-(f) are 33.46, 32.79, 33.95, 33.63 and 34.29 dB, respectively.

The f is the forward mapping function of GCESS network, including parallel implement of GCN and CNN. $\mathbf{\Theta}$ is the parameters of GCESS. $\mathbf{x}_u = \mathbf{F}_u^H \mathbf{y}$ is the zero-filled reconstruction. The flowchart of our proposed network is shown in Fig. 5. Graph Convolutional Network (GCN) combined with CNN to constitute GCESS module. The undersampled image $\mathbf{x}_u$ is the input of the integrative network. Before $\mathbf{x}_u$ enters the GCN module of block 1, a SPIRiT-based pre-reconstructed image is obtained to learn similar weight by Gtrans.

With graph convolution, non-local similarity information can be extracted from the adjacency matrix as Fig. 1 showing. Additionally, CNN focus on representing pixel-level fine and coarse features and is incorporated to reconstruct image. It can be seen from the Fig. 5 that when the image is filtered by spatial convolution, the details of the image paches have been reconstructed, so that the information of all image paches is well reconstructed. At the same time, while the graph convolution is reconstructing the image, it further uses the most similar image paches scattered in the grid image range of the target image patch to further restore the target one. The Itrans put graphs node features back into MRI images canvas to carry out GCN reconstruction, and combine with reconstructed result of CNN to form GCESS. The ResNet[10] adds the input to the neural networks preliminary result of GCESS, following by a DC module.

The sampled partial k-space data have been acquired so that network don't have the necessary to reconstruct. DC using the sampled k-space data wisely will enhance the data fidelity[22]:

$$\hat{\mathbf{k}} = (\mathbf{1}_H - \mathbf{H}) \mathrm{e}\ \hat{\mathbf{k}} + \lambda \mathbf{k}_u, \tag{12}$$

where $\hat{\mathbf{k}}$ is the reconstructed k-space data corresponding to reconstructed image. $(\mathbf{1}_H - \mathbf{H})$ strands for the inverse undersampling pattern. e represents the multiplication of corresponding elements in the matrix. $\mathbf{k}_u$ denotes the k-space data which is acquired from coils. The acquisition of k-space from the coils is not noise free. Thus, the λ is used to balance the k-space data fidelity between sampled data and the reconstructed k-space data from the network. DC is realized by replacing the k-th predicted data with the original k-space data if it has been sampled. To obtain the forward pass of the layer performing data consistency in k-space:

$$f_{dc}\left(\hat{\mathbf{x}}, \mathbf{k}_u, \lambda\right) = \sum_{j}^{J} \mathbf{C}_j^H \mathbf{F}^{-1}\left(\mathbf{F}\mathbf{C}_j \hat{\mathbf{x}} + \lambda \mathbf{k}_u\right). \tag{13}$$

We set λ to a very small value ($\lambda = 1 - 1\times10^{-6}$) to ensure that the collected data is fully fidelity meanwhile the noise is well suppressed.

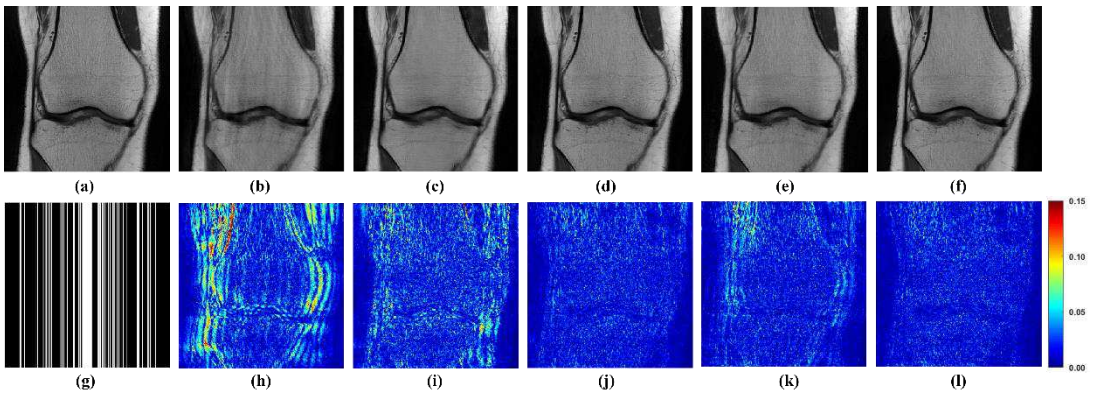

Fig. 8. The proposed GCESS network compared with state-of-the-art MRI reconstruction methods. (a) is the fully sampled image. The experiments correspond to a 1D Cartesian sampling with AF=4 as shown in (g). (b)-(f) are the images of reconstructed results by SPIRiT, Unet, DCCNN, MoDL, and GCESS, respectively. (h)-(l) are the corresponding error maps. The PSNR of (b)-(f) are 28.68, 30.73, 34.05, 32.83 and 34.69 dB, respectively.

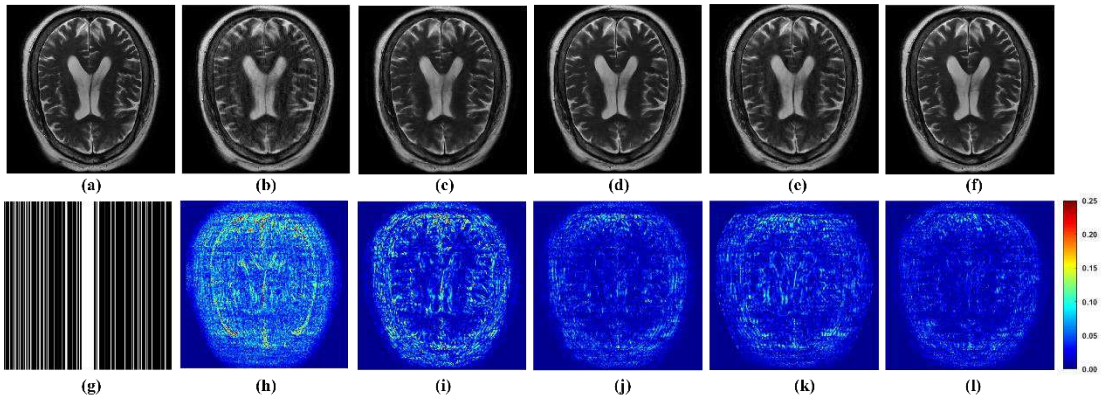

Fig. 9. The proposed GCESS network compared with state-of-the-art MRI reconstruction methods. (a) is the fully sampled image. The experiments correspond to a 1D Cartesian sampling with AF=4 as shown in (g). (b)-(f) are the images of reconstructed results by SPIRiT, Unet, DCCNN, MoDL, and GCESS, respectively. (j)-(j) are the corresponding error maps. The PSNR of (b)-(f) are 28.67, 29.44, 33.33, 32.15 and 34.61 dB, respectively.

Result

Experiments are implemented in Python 3 using PyTorch as the backend. Training, validation, and testing were performed on a seventh-generation Intel Core i7 processor with 32 GB of RAM and an RTX 3090 GPU (24 GB memory).

Datasets

This paper uses two datasets: the knee dataset of variational network (VN) [20] and the fastMRI[37] brain dataset, both from open repositories. The coil sensitivity maps were estimated from the central k-space region of each slice using ESPIRiT[38].

The public knee dataset provided by VN [20] are used in our experiments to evaluate the performance of the proposed method. It is coronal density weighted k-space data acquired from a 2D turbo-spin echo sequence at a 3T MRI system with 15 coils (Siemens Magnetom Skyra). There are 20 subjects and each subject contains about 35 slices. For each subject used for the experiment, we all selected the middle twenty slices of size 256×256. Fourteen subjects were used for training, two for validation, and the remaining for the test.

We used multi-coil T2 weighted k-space data of the fastMRI[37] open dataset. There are 45 subjects and contains about 427 slices. For each subject used for the experiment,

we all selected the middle twenty slices of size 320×320. The training slice is 296, 36 for validation, and the remaining for the test.

Table 2. Quantitative results (RLNE, PSNR, and SSIM) of the compared method (Mean ± standard).

Knee dataset				
Pattern	Method	RLNE×100	SSIM×100	PSNR
1D Cartesian AF=4	SPIRiT	10.10 ± 1.16	81.75 ± 1.97	28.32 ± 0.98
	Unet	9.02 ± 1.29	80.88 ± 3.66	29.36 ± 1.00
	DCCNN	5.86 ± 0.94	88.20 ± 1.87	33.14 ± 1.36
	MoDL	7.01 ± 0.97	85.81 ± 3.15	31.56 ± 1.19
	GCESS	**5.10 ± 0.88**	**89.94 ± 2.39**	**34.19 ± 1.52**
2D Random AF=8	SPIRiT	6.32 ± 0.69	83.13 ± 1.55	32.41 ± 1.13
	Unet	9.44 ± 1.14	74.36 ± 5.67	28.95 ± 1.24
	DCCNN	5.21 ± 0.80	87.46 ± 3.03	34.16 ± 1.80
	MoDL	4.87 ± 0.75	86.78 ± 3.67	34.86 ± 1.90
	GCESS	**4.69 ± 0.76**	**88.12 ± 3.34**	**35.09 ± 1.93**
2D Random AF=10	SPIRiT	6.90 ± 0.67	80.45 ± 2. 01	31.65 ± 1.10
	Unet	9.81 ± 1.29	72.38 ± 6.35	28.63 ± 1.31
	DCCNN	5.67 ± 0.88	85.06 ± 3.77	33.42 ± 1.81
	MoDL	6.13 ± 0.78	83.05 ± 3.90	32.70 ± 1.57
	GCESS	**5.22 ± 0.85**	**85.39 ± 4.15**	**34.16 ± 1.94**
Brain dataset				
Pattern	Method	RLNE×100	SSIM×100	PSNR
1D Cartesian AF=4	SPIRiT	14.90 ± 1.93	85.24 ± 2.41	29.83 ± 0.64
	Unet	13.06 ± 1.16	90.54 ± 1.69	30.94 ± 0.91
	DCCNN	8.48 ± 1.14	94.62 ± 1.29	34.73 ± 1.02
	MoDL	12.17 ± 5.20	90.79 ± 4.26	32.01 ± 2.82
	GCESS	**7.57 ± 1.17**	**95.36 ± 1.27**	**35.73 ± 1.14**

Note: The lowest RLNE, highest PSNR and SSIM values are bold faced.

Network

As Fig. 5 showing, 10 iteration blocks that have 2 GCNs and 4 CNNs layers with a Batch Normalization (BN) of each layer are connected sequentially to build the whole network. CNN consist of four layers and each layer contains 64 filters whose size is 3×3. Gtrans is the operator to construct images to graph. Graph node features will be the input of GCN. Itrans is the inverse operator of Gtrans, in which output features will be put back to canvas to be the reconstructed image. The models in our experiment were trained 100 epochs. All filters are initialized by using "normal" initialization[39], and Adam[40] is selected as the optimizer in the training progress with a learning rate of 0.0015.

The first step in computing the adjacency matrix is to calculate the Gaussian distance as the difference between each image patch. The calculation of Gaussian distance is a long process. Therefore, the adjacency matrix update during training leads to time-consuming. The time to calculate one adjacency matrix of 256×256 image each is 4.6s and each of 320×320 image is 9.6s. However, the non-local information in the undersampled parallel MRI images is inaccurate. To solve these problems, we use SPIRiT as pre-reconstruction method to fix non-local information extracted from the graph. The reconstructions time of SPIRiT is 15.8s. The training time of GCESS is 11.2h while the reconstructing time is 0.14s (Exinclude computing adjacency matrix and pre-reconstruction time).

Evaluation Criteria

To evaluate the image reconstruction quality of all compared methods in an objective view, we use RLNE[5], structure similarity index measure (SSIM)[41], and the peak signal-to-noise ratio (PSNR) as the quantitative criteria. The RLNE is defined in eq. (10).

The SSIM is defined as:

$$SSIM = \frac{\left(2\mu_{\mathbf{x}}\mu_{\hat{\mathbf{x}}} + C_1\right)\left(2\sigma_{\mathbf{x}\hat{\mathbf{x}}} + C_2\right)}{\left(\mu_{\mathbf{x}}^2 + \mu_{\hat{\mathbf{x}}}^2 + C_1\right)\left(\sigma_{\mathbf{x}}^2 + \sigma_{\hat{\mathbf{x}}}^2 + C_2\right)}, \tag{14}$$

where $\mu_{\mathbf{x}}$ and $\mu_{\hat{\mathbf{x}}}$ denote the means of $\mathbf{x}$ and $\hat{\mathbf{x}}$, $\sigma_{\mathbf{x}}$ and $\sigma_{\hat{\mathbf{x}}}$ is the standard deviations of $\mathbf{x}$ and $\hat{\mathbf{x}}$, and $\sigma_{\mathbf{x}\hat{\mathbf{x}}}$ is the covariance of $\mathbf{x}$ and $\hat{\mathbf{x}}$. C_1, C_2 is a constant to maintain stability close to zero.

The PSNR is defined as:

$$PSNR(dB) = 10 \cdot \log_{10}\left(\frac{PQ\|\mathbf{x}\|_{\infty}}{\|\mathbf{x}-\hat{\mathbf{x}}\|_2}\right), \tag{15}$$

P and Q represent the dimension of the frequency encoding and phase encoding, respectively.

The lower reconstruction error with the lower RLNE indicates higher consistencies between reconstructed and fully sampled images. Higher PSNR means better signal-to-noise ratio, and higher SSIM values indicate better detail preservation and fewer image distortions in the reconstruction.

Comparison with existing methods

The MRI reconstruction using the proposed GCESS is compared with other three deep learning methods and one conventional method. The conventional method used for comparative experiments is SPIRiT[31]. We test the parameters of SPIRiT to make the algorithm perform its best on the dataset we are using. The testing result shows that it adopted the parameter calibration kernel size 3×3 and Tikhonov regularization in the calibration was set to be 10^{-3}. Tikhonov regularization in the reconstruction was set for 10^{-5} implementing SPIRiT, which took 30 iterations. The other three deep learning methods are IUNET[42], DCCNN[22] and MoDL[19]. IUNET[42] is the baseline of MRI image reconstruction. DCCNN is one of the earliest methods to apply deep learning to MRI reconstruction. The number of CNN layers in each layer is 6 and the number of iterations is 5, which is consistent with the original paper. To be fair, we added a BN layer to each layer of CNN to optimize the entire network. MoDL[19] is a classic model-driven approach in deep learning MRI reconstruction framework in recent years. The forward layers and backward layers of CNN both contain 64 filters which size is 3×3. Since the performance of MoDL saturates around 8-10 iterations, we used this typical setting in the experiment. Each iteration has 4 CNN layers with 64

filters per layer which size is 3×3.

To evaluate the performance of the proposed method, one-dimensional (1D) Cartesian undersampling pattern and two-dimensional (2D) random undersampling are adopted. The reconstructed images and corresponding error maps of the compared methods with different acceleration factors are shown in Fig. 6-9. From the reconstruction errors in Fig. 6-9, the SPIRiT and the IUNET have obvious artifacts as shown in Fig. 6-9 (b). MoDL shows better artifacts suppression ability than DCCNN, and the proposed GCESS suppresses artifacts best. Comparing errors in Fig. 6(c)-(d) to Fig. 7(c)-(d), it shows that, with the increase of acceleration factor the reconstruction results of MoDL deteriorate faster than those of the proposed GCESS.

The average numerical performance with standard deviations of the testing knee datasets of the proposed method and state-of-the-art methods are summarized in Table 2. The Table 2 shows quantitative values for 2D random undersampling pattern AF=8 and 10 for different methods and 1D Cartesian undersampling pattern AF=4 for different methods. It can be observed that PSNR, SSIM, and RLNE values of GCESS from the mean show the best reconstructed results.

Ablation Studies

To verify the effectiveness of the proposed integrated network can extract both non-local and local information, we conduct ablation experiments to test the effects of several important components in the network proposed.

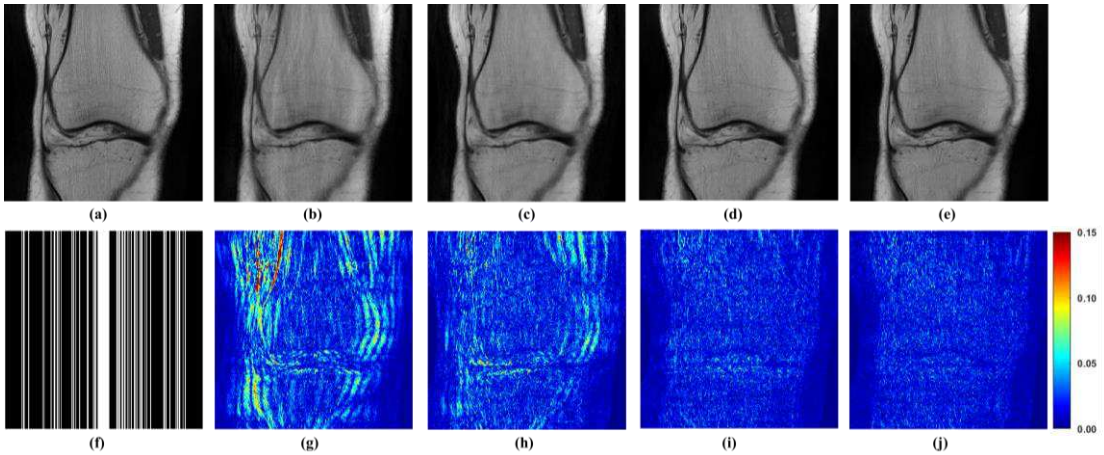

Fig. 10. Ablation studies results of the proposed GCESS network. (a) is the fully sampled image. (f) is the 1D Cartesian undersampling pattern with AF=4. (b)-(e) are the images of

reconstructed results by SPIRiT, GCN, CNN, and GCESS, respectively. (g)-(j) are the corresponding error maps. The PSNR of (h)-(e) are 29.63 ,31.69, 34.51 and 34.95 dB, respectively.

We remove the graph convolution from GCESS to obtain CNN for MRI reconstruction. Similarly, we remove the convolutional neural network from GCESS to obtain GCN (the same as GCN in SectionII.D). Fig. 10 shows the reconstructed result with 1D Cartesian undersampling pattern AF=4. In Fig. 10, GCN provide the image with nice artifacts suppression. The GCESS compared with the global error of CNN with a significant improvement. By integrating both non-local and local information, GCESS extra promotion in quantitative results. The Table 3 gives the quantitative results of the whole test dataset with 1D Cartesian undersampling pattern AF=4. GCESS has better metrics than the other two networks across-the-board values.

Table3. Quantitative results (RLNE, PSNR, and SSIM) of the compared method (Mean ± standard).

Method	RLNE×100	SSIM×100	PSNR
GCN	8.55 ± 0.81	84.39 ± 2.82	29.78 ± 0.91
CNN	5.72 ± 1.13	89.21 ± 2.68	33.39 ± 1.69
GCESS	$\mathbf{5.19 \pm 0.88}$	$\mathbf{89.94 \pm 2.39}$	$\mathbf{34.19 \pm 1.52}$

Note: The lowest RLNE, highest PSNR and SSIM values are bold faced.

Discussion

This work focusses on the GCESS network for MRI reconstructions. The network structure not only inherits the extracting local information advantage of CNN but also utilizes GCN to make full use of non-local information to eliminate artifacts. Local spatial convolutional operations on grid-like data cannot capture non-local self-similarity information due to the locality of convolutional kernels. To extract non-local information, we construct MRI image into graph to enhance the connection between image patches. The non-local information can enhance connected relations between image patches which does not adjoin in the grid-like data but shares lots of structure information. After constructing the graph, MRI reconstructions are regarded as node (patch) reconstruction using GCN.

Our method also have limitations. The first step of constructing the graph is finding the eight most similar image patches for each patch. This process must calculate the Gaussian distance as the similarity between patches (Time-consuming 8.6s). Although we have tried numerous sorts of methods like stacking image patches or using GPU to speed up computation, the problem of time-consuming still exists. Because of the above time reasons, it is difficult to update the graph after every epoch of the training process. Thus, we use SPIRiT as our pre-reconstruct method to fix non-local information extracted from image. To meet the time requirement of clinical practice, a more computationally efficient method or an embedded graph learning network is to be further developed. This will be considered in our next work.

Conclusions

In this work, Graph Convolution network with Enhanced Self-Similarity (GCESS) is proposed which attempt to combine non-local self-similarity information and local information for MRI reconstruction. Local information is introduced in a common way as a convolutional neural network. The non-local self-similarity is represented by the graph, followed by a graph filtering process. As the network training, self-similarities will be enhanced and graph convolution filter will be updated. The enhanced self-similarity information then guides the image reconstruction by fusing the non-local information passed through enhanced graph edges. This process incorporates additional non-local similarity information within the target patch and makes better artifact suppression and edge preserving. Experimental in vivo datasets show that the proposed network enables better reconstruction results than the state-of-the-art methods. Notably, the proposed methods allow reconstructions with smaller errors, and with better details and fine structures.

Declarations

Acknowledgments

Not applicable

Funding

This work is supported in part by the National Natural Science Foundation of China (61901188, 62122064, 61971361, and 61871341), the Natural Science Foundation of Fujian Province of China (2022J05163), and the Science and Technology Fund of Fujian Education Department (JT180280).

Availability of data and materials

The data used in this paper are public datasets.

Abbreviations

MRI: magnetic resonance imaging; GCESS: graph convolution network with enhanced self-similarity; GCN: graph convolutional network; CNN: convolutional neural network; Gtrans: graph transformer; DC: data consistency; UnGCN: GCN with undersampled similarity; RecGCN: GCN with reconstructed image; RLNE: relative ℓ_2 norm error; SSIM: sructure similarity index measure; PSNR: the peak signal-to-noise ratio.

Authors' contributions

ZL designed and guided the implement of the GCESS MRI reconstruction method together with XQ, QM implemented this method. ZL and QM contribute equally to this work. Algorithm development and data analysis were carried out by ZL, QM, ZW, YQ, HZ, BQ and XQ. All authors have been involved in drafting and revising the manuscript and approved the final version to be published. All authors read and approved the final manuscript.

Ethics approval and consent to participate

The data used in this paper are publicly available as described in VN[20] and fastMRI[37]. Informed consents were obtained from the subjects.

Consent for publication

Not applicable.

Competing interests

The authors declare that they have no competing interests.

Publisher's Note

Open Access

References

1. Lustig M, Donoho D, Pauly JM: **Sparse MRI: The application of compressed sensing for rapid MR imaging**. *Magn Reson Med* 2007, **58**(6):1182-1195.
2. Hamilton J, Franson D, Seiberlich N: **Recent advances in parallel imaging for MRI**. Prog Nucl Magn Reson Spectrosc 2017, **101**:71-95.
3. Chen Y, Ye X, Huang F: **A novel method and fast algorithm for MR image reconstruction with significantly under-sampled data**. Inverse Problems & Imaging 2010, **4**(2):223.
4. Ravishankar S, Bresler Y: **MR image reconstruction from highly undersampled k-space data by dictionary learning**. IEEE Trans Med Imaging 2011, **30**(5):1028-1041.
5. Qu X, Guo D, Ning B, Hou Y, Lin Y, Cai S, Chen Z: **Undersampled MRI reconstruction with patch-based directional wavelets**. Magn Reson Imaging 2012, **30**(7):964-977.
6. Lai Z, Qu X, Liu Y, Guo D, Ye J, Zhan Z, Chen Z: **Image reconstruction of compressed sensing MRI using graph-based redundant wavelet transform**. Med Image Anal 2016, **27**:93-104.
7. Liang D, Wang H, Chang Y, Ying L: **Sensitivity encoding reconstruction with nonlocal total variation regularization**. Magn Reson Med 2011, **65**(5):1384-1392.
8. Zhang X, Lu H, Guo D, Lai Z, Ye H, Peng X, Zhao B, Qu XJapa: **Accelerated MRI reconstruction with separable and enhanced low-rank hankel regularization**. IEEE Trans Med Imaging 2022;41(9):2486-98.
9. Ronneberger O, Fischer P, Brox T: **U-net: Convolutional networks for biomedical image segmentation**. In: *International Conference on Medical image computing and computer-assisted intervention: 2015*: Springer; 2015: 234-241.
10. He K, Zhang X, Ren S, Sun J: **Deep residual learning for image recognition**. In: *Proceedings of*

the IEEE conference on computer vision and pattern recognition: 2016; 2016: 770-778.

11. Ren S, He K, Girshick R, Sun J: **Faster R-CNN: Towards real-time object detection with region proposal networks**. IEEE Trans Pattern Anal 2017, **39**(6):1137-1149.
12. Wang S, Su Z, Ying L, Peng X, Zhu S, Liang F, Feng D, Liang D: **Accelerating magnetic resonance imaging via deep learning**. In: *2016 IEEE 13th international symposium on biomedical imaging (ISBI): 2016*: IEEE; 2016: 514-517.
13. Zhu B, Liu JZ, Cauley SF, Rosen BR, Rosen MS: **Image reconstruction by domain-transform manifold learning**. *Nature* 2018, **555**(7697):487-492.
14. Knoll F, Hammernik K, Zhang C, Moeller S, Pock T, Sodickson DK, Akcakaya MJapa: **Deep learning methods for parallel magnetic resonance image reconstruction**. IEEE Signal Process Mag 2020;37(1):128-40.
15. Wang Z, Qian C, Guo D, Sun H, Li R, Zhao B, Qu X: **One-dimensional deep low-rank and sparse network for accelerated MRI**. IEEE Trans Med Imaging DOI:10.1109/TMI.2022.3203312, 2022.
16. Lu T, Zhang X, Huang Y, Guo D, Huang F, Xu Q, Hu Y, Ou-Yang L, Lin J, Yan ZJJoMR: **pFISTA-SENSE-ResNet for parallel MRI reconstruction**. J Magn Reson 2020;318:106790.
17. Souza R, Bento M, Nogovitsyn N, Chung KJ, Loos W, Lebel RM, Frayne R: **Dual-domain cascade of U-nets for multi-channel magnetic resonance image reconstruction**. Magn Reson Imaging 2020;71:140-53.
18. Arshad M, Qureshi M, Inam O, Omer H: **Transfer learning in deep neural network based under-sampled MR image reconstruction**. Magn Reson Imaging 2021;76:96-107.
19. Aggarwal HK, Mani MP, Jacob MJItomi: **MoDL: Model-based deep learning architecture for inverse problems**. IEEE Trans Med Imaging 2018;38(2):394-405.
20. Hammernik K, Klatzer T, Kobler E, Recht MP, Sodickson DK, Pock T, Knoll F: **Learning a variational network for reconstruction of accelerated MRI data**. Magn Reson Med 2018;79(6):3055-71.
21. Wang Z, Fang H, Qian C, Shi B, Bao L, Zhu L, Zhou J, Wei W, Lin J, Guo D: **A faithful deep sensitivity estimation for accelerated magnetic resonance imaging**. arXiv preprint arXiv:221012723 2022.
22. Schlemper J, Caballero J, Hajnal JV, Price A, Rueckert D: **A deep cascade of convolutional neural networks for MR image reconstruction**. In: *International Conference on Information Processing in Medical Imaging: 2017*: Springer; 2017: 647-658.
23. Yang Q, Wang Z, Guo K, Cai C, Qu X: **Physics-driven synthetic data learning for biomedical magnetic resonance**. IEEE Signal Process Mag DOI: 10.1109/MSP.2022.3183809, 2022.
24. Feng C-M, Yang Z, Fu H, Xu Y, Yang J, Shao L: **DONet: dual-octave network for fast MR image reconstruction**. IEEE T NEUR NET LEAR 2021.
25. Ramanarayanan S, Murugesan B, Ram K, Sivaprakasam M: **DC-WCNN: A deep cascade of wavelet based convolutional neural networks for MR Image Reconstruction**. In *2020 IEEE 17th International Symposium on Biomedical Imaging (ISBI)*, pp. 1069-1073.
26. Welling M, Kipf TN: **Semi-supervised classification with graph convolutional networks**. In: *J International Conference on Learning Representations (ICLR 2017): 2016*; 2016.
27. Zhou S, Zhang J, Zuo W, Loy CCJapa: **Cross-scale internal graph neural network for image super-resolution**. 2020.
28. Han K, Wang Y, Guo J, Tang Y, Wu E: **Vision GNN: An image is worth graph of nodes**. *arXiv preprint arXiv:220600272* 2022.

29. Rey S, Segarra S, Heckel R, Marques AG: **Untrained graph neural networks for denoising**. *arXiv preprint arXiv:210911700* 2021.
30. Shen Y, Li H, Yi S, Chen D, Wang X: **Person re-identification with deep similarity-guided graph neural network**. In: *Proceedings of the European conference on computer vision (ECCV): 2018*; 2018: 486-504.
31. Lustig M, Pauly JM: **SPIRiT: iterative self‐consistent parallel imaging reconstruction from arbitrary k‐space**. Magn Reson Med 2010;64(2):457-71.
32. Liu B, Sebert F, Zou Y, Ying L: **SparseSENSE: randomly-sampled parallel imaging using compressed sensing**. In: *In: Proceedings of the 16th Annual Meeting of ISMRM: 2008*: Citeseer; 2008.
33. Ram I, Elad M, Cohen I: **Generalized tree-based wavelet transform**. IEEE Trans Signal Proces 2011;59(9):4199-209.
34. Ram I, Elad M, Cohen I: **Image processing using smooth ordering of its patches**. IEEE Trans Signal Process 2013;22(7):2764-74.
35. Osher S, Shi Z, Zhu W: **Low dimensional manifold model for image processing**. SIAM Journal on Imaging Sciences 2017;10(4):1669-90.
36. Hammond DK, Vandergheynst P, Gribonval R: **Wavelets on graphs via spectral graph theory**. Appl Comput Harmon Anal 2011;30(2):129-50.
37. Zbontar J, Knoll F, Sriram A, Murrell T, Huang Z, Muckley MJ, Defazio A, Stern R, Johnson P, Bruno M: **fastMRI: An open dataset and benchmarks for accelerated MRI**. *arXiv preprint arXiv:181108839* 2018.
38. Uecker M, Lai P, Murphy MJ, Virtue P, Elad M, Pauly JM, Vasanawala SS, Lustig MJMrim: **ESPIRiT—an eigenvalue approach to autocalibrating parallel MRI: where SENSE meets GRAPPA**. Magn Reson Med 2014;71(3):990-1001.
39. Glorot X, Bengio Y: **Understanding the difficulty of training deep feedforward neural networks**. In: *Proceedings of the thirteenth international conference on artificial intelligence and statistics: 2010*: JMLR Workshop and Conference Proceedings; 2010: 249-256.
40. Kingma DP, Ba J: **Adam: A method for stochastic optimization**. *arXiv preprint arXiv:14126980* 2014.
41. Wang Z, Bovik AC, Sheikh HR, Simoncelli EP: **Image quality assessment: from error visibility to structural similarity**. IEEE Trans Image Process 2004;13(4):600-12.
42. Ye JC, Han YS: **Deep convolutional framelets: A general deep learning for inverse problems**. SIAM Journal on Imaging Sciences 2017, **11**(2).